Title

Reversibly disulfide cross-linked micelles improve the pharmacokinetics and facilitate the targeted, on-demand delivery of doxorubicin in the treatment of B-cell lymphoma

Journal

Nanoscale, 10(17)

ISSN

2040-3364

Authors

Xiao, Kai

Liu, Qiangqiang

Al Awwad, Nasir

et al.

Publication Date

2018-05-03

DOI

10.1039/c8nr00680f

Peer reviewed

HHS Public Access

Author manuscript

Nanoscale. Author manuscript; available in PMC 2019 May 03.

Published in final edited form as:

Nanoscale. 2018 May 03; 10(17): 8207–8216. doi:10.1039/c8nr00680f.

Reversibly disulfide cross-linked micelles improve the pharmacokinetics and facilitate the targeted, on-demand delivery of doxorubicin in the treatment of B-cell lymphoma

Kai Xiao[a,*], **Qiangqiang Liu**[a,b], **Nasir Al Awwad**[b,e], **Hongyong Zhang**[c], **Li Lai**[a], **Yan Luo**[b], **Joyce S. Lee**[b,d], **Yuanpei Li**[b,*], and **Kit S. Lam**[b,c,*]

[a]National Chengdu Center for Safety Evaluation of Drugs, State Key Laboratory of Biotherapy, Collaborative Innovation Center for Biotherapy, West China Hospital, Sichuan University, Chengdu 610041, P.R. China

[b]Department of Biochemistry & Molecular Medicine, UC Davis Cancer Center, University of California Davis, Sacramento, CA 95817, USA

[c]Division of Hematology & Oncology, Department of Internal Medicine, School of Medicine, University of California Davis, CA 95817, USA

[d]Department of Pharmacy, University of California, Davis Medical Center, Sacramento, CA 95817, USA

[e]Department of Clinical Pharmacy, Faculty of Clinical Pharmacy, Albaha University, Albaha, 65431, Saudi Arabia

Abstract

Doxorubicin (DOX) is commonly used to treat human malignancies, and its efficacy can be maximized by limiting the cardiac toxicity when combined with nanoparticles. Here, we reported a unique type of reversibly disulfide cross-linked micellar formulation of DOX (DOX-DCMs) for the targeted therapy of B-cell lymphoma. DOX-DCMs exhibited high drug loading capacity, optimal particle sizes (15–20 nm), outstanding stability in human plasma, and stimuli-responsive drug release profile under reductive conditions. DOX-DCMs significantly improved the pharmacokinetics of DOX, and its elimination half-life ($t_{1/2}$) and area under curve (AUC) were 5.5 and 12.4 times of that of free DOX, respectively. Biodistribution studies showed that DOX-DCMs were able to preferentially accumulate in the tumor site and significantly reduce the cardiac uptake of DOX. In a xenograft model of human B-cell lymphoma, compared with the equivalent dose of free DOX and non-crosslinked counterpart, DOX-DCMs not only significantly inhibited the tumor growth, prolonged the survival rate, but also remarkably reduced DOX-associated cardiotoxicity. Furthermore, the exogenous administration of N-acetylcysteine (NAC) at 24 h further improved the therapeutic efficacy of DOX-DCMs, which provides a “proof-of-concept” for precise drug delivery on-demand, and may have great translational potential as future cancer nano-therapeutics.

Graphical abstract

*Corresponding authors. xiaokaikaixiao@scu.edu.cn; lypli@ucdavis.edu; kslam@ucdavis.edu e.

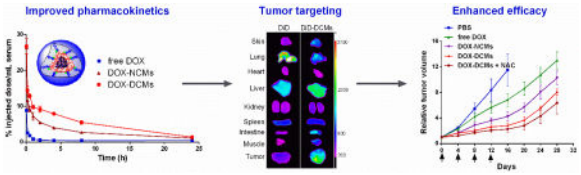

Disulfide cross-linked micellar formulation significantly improved the pharmacokinetics, tumor targeting, and anti-tumor efficacy of doxorubicin against B-cell lymphoma.

Keywords

stimuli responsive; crosslinked micelles; doxorubicin; B-cell lymphoma; drug delivery

Introduction

Doxorubicin (DOX) is a highly potent chemotherapeutic agent, and commonly used in the standard CHOP (cyclophosphamide, DOX, vincristine, and prednisone) regimen for the treatment of non-Hodgkin lymphoma [1]. It kills cells through intercalation of DNA and inhibition of topoisomerase II [2]. Unfortunately, its clinical use is limited by its short half-life, nonspecific distribution, and serious toxicities including myelosuppression, and cardiotoxicity manifested by congestive cardiomyopathy [3].

Nanotechnology has shown great promise in addressing these limitations by selectively delivering drugs to the site of disease such as cancer, and is able to reduce the side effects and improve the therapeutic efficacy [4]. Various nanoparticle-based drug delivery systems including liposomes [5], inorganic nanoparticles [6], dendrimers [7], micelles [8], and protein aggregates [9], have been recently developed for the delivery of chemotherapeutics agents, which are generally believed to be able to prolong the blood circulation, passively accumulate at tumor site with reduced distribution in normal tissues *via* the enhanced permeability retention (EPR) effect [10]. Doxil®, a liposomal formulation of DOX, is in fact the first nano-drug originally approved by U.S. Food and Drug Administration (FDA) in 1995 for the treatment of AIDS-related Kaposi sarcoma [11]. Although the liposomal formulation significantly reduces the DOX-related cardiotoxicity, its anti-cancer efficacy is only marginally improved in clinical practice [12, 13]. This may be due in part to its relatively large particle size (approx. 140 nm), thus obviating the EPR effect, and limiting intra-tumoral penetration and diffusion [14]. Polymer micelles may provide greater therapeutic advantage than liposomes, because their size can be significantly smaller, which makes micelles more effective in targeting tumor [15]. In addition, polymeric micelles generally have superior biocompatibility, high capacity to encapsulate hydrophobic drugs, and favorable drug release profiles [16].

We have recently reported a series of new telodendrimer (linear-dendritic block copolymer) comprising polyethylene glycol (PEG) and cholic acids (CA) [15, 17–26], which were successfully applied to the targeted delivery of chemotherapeutic drugs such as paclitaxel [17, 20, 23], DOX [21], and vincristine [24]. For example, PEG^{2k}-CA_4 telodendrimer was found to be able to efficiently encapsulate DOX, and the corresponding micellar formulation

significantly prolonged the blood retention time, enhanced the tumor accumulation, improved the anti-cancer efficacy, and reduced the cardiac toxicity of DOX in B-cell lymphoma xenograft models [21].

Although PEG^{2k}-CA_4 telodendrimer has shown great potential for the delivery of DOX in previous studies, our latest research found that it may cause hemolysis of red blood cells (Figure S-1). In addition, colloidal instability of PEG^{2k}-CA_4 micelles is another concern for the further clinical development. Because of the thermodynamic properties of polymeric micelles, interactions with plasma proteins or other biomacromolecules in the body may potentially disrupt the equilibrium between micelles and unimers, resulting in early dissociation of micelles and premature release of drugs[27]. To slove these potential problems, we recently introduced thiol group into the telodendrimer (PEG^{5k}-Cys_4-L_8-CA_8) to prepare reversibly disulfide cross-linked micelles (DCMs) [20]. The intra-micellar disulfide crosslinkages could minimize the early drug release in blood circulation, and could be cleaved by the elevated levels of glutathione (GSH) in tumor cells [20]. Meanwhile, as shown in supplementary Figure S-1, the intramicellar disulfide cross-linkages were able to completely prevent the potential hemolytic properties of the non-crosslinked PEG^{5k}-CA_8 micelles and PEG^{2k}-CA_4 micelles. Furthermore, we have proved that DCMs can efficiently deliver both chemotherapeutic drugs (*e.g.* paclitaxel, vincristine) and molecularly targeted drugs (*e.g.* histone deacetylase inhibitor Thailandepsin A) into tumor sites, resulting in superior anti-cancer efficacy in xenograft models of ovarian cancer, lymphoma, and breast cancer [20, 24, 28].

In the present study, we aimed to encapsulate DOX into the newly developed redox-responsive DCMs and facilitate the targeted, on-demand delivery of DOX to B-cell lymphoma. The physicochemical properties of DOX-loaded DCMs (DOX-DCMs) were fully characterized, including drug loading capacity, morphology, particle size, stability, and drug release profile. The *in vitro* cytotoxicity of DOX-DCMs against B-cell lymphoma cells was measured by MTS assay. The *in vivo* pharmacokinetics, biodistribution, and tumor targeting of DCMs loaded with DOX drug or DiD fluorescence dye were investigated by both DOX fluorescence measurement and near infrared fluorescence (NIRF) optical imaging approach, respectively. Finally, the anti-tumor effect and toxicity of DOX-DCMs were evaluated in a xenograft model of human B-cell lymphoma, and compared with free DOX and non-crosslinked counterparts.

2. Materials and Methods

2.1 Materials

DOX powder was purchased from Selleckchem (Houston, TX, USA). Monomethylterminated poly(ethylene glycol) monoamine (MeO-PEG-NH2, MW: 5000 Da) was purchased from Rapp Polymere (Tuebingen, Germany). (Fmoc)Lys(Fmoc)-OH was obtained from AnaSpec Inc. (San Jose, CA, USA). 1,10-Dioctadecyl-3,3,30,30-tetramethylindodicarbocyanine perchlorate (DiD, D-307) and 4', 6-diamidino-2-phenylindole (DAPI) were purchased from Life Technologies (Grand Island, NY, USA). CellTiter 96® AQueous Non-Radioactive Cell Proliferation Assay (MTS) kit was purchased

from Promega (Madison, WI, USA). Cholic acid, sodium dodecyl sulfate (SDS), GSH, NAC, and other chemicals were purchased from Sigma-Aldrich (St. Louis, MO, USA).

2.2 Preparation and characterization of DOX-DCMs

PEG^{5k}-CA_8 telodendrimer and PEG^{5k}-Cys_4-L_8-CA_8 telodendrimer were synthesized *via* solution-phase condensation reactions as described previously [17, 20]. DOX-loaded non-crosslinked micelles (DOX-NCMs) or DOX-DCMs were prepared by the solvent evaporation method as described previously [17, 20]. Briefly, DOX was neutralized with 3 molar equivalent of trimethylamine, mixed with PEG^{5k}-CA_8/PEG^{5k}-Cys_4-L_8-CA_8 telodendrimer in methanol/chloroform (1:1, v/v). This organic solvent was evaporated to form a thin film, followed by the hydration with PBS buffer. DOX-DCMs were obtained by crosslinking the intramicellar disulfide bonds *via* the addition of 1.5 equivalent H_2O_2[20]. Drug loading of DOX-NCMs and DOX-DCMs were measured by DOX fluorescence detection using NanoDrop 2000 spectrophotometer (Thermo Scientific). To visualize the *in vivo* biodistribution and tumor targeting of DCMs, DiD (near infrared fluorescence dye) as a drug surrogate was loaded into DCMs to prepare DiD-DCMs with the final concentration of 0.5 mg/mL.

The size and morphology of DOX-DCMs (1 mg/mL) were detected by dynamic light scattering (DLS) and Philips CM-120 transmission electron microscopy (TEM), respectively. The stability of DOX-DCMs was analyzed by DLS monitoring the size changes under physiological (human plasma, 37 °C) and micelle-disrupting conditions (SDS, 2.5 mg/mL) [29] at predetermined time intervals. In addition, the stability in particle size of DOX-DCMs in the presence of both SDS and reducing agent (GSH 10 mM, or NAC 10 mM) was also measured.

The drug release characteristicsfrom DOX-DCMs were measured by the dialysis method as describe previously [17]. Briefly, dialysis cartridges with the molecular weight cutoff of 3.5 kDa were infilled with aliquots of various DOX formulations, and dialyzed againt PBS with activated charcoal at 37 °C. The remaining DOX concentration in the dialysis cartridge was measured by spectrophotometry at different time points. In addition, the drug release characteristics of DOX-DCMs under reducing conditions were measured by the addition of GSH (10 mM) or NAC (10 mM).

2.3 Cell culture and animals

Raji and Ramos B-cell lymphoma cell lines were purchased from American Type Culture Collection (ATCC; Manassas, VA, USA), and maintained in RPMI-1640 medium with 10% FBS at 37 ºC in a humidified 5% CO_2 incubator.

Female nude mice (6–8 weeks) were purchased from Harlan (Livermore, CA), and bred in accordance with Association for Assessment and Accreditation of Laboratory Animal Care (AAALAC) guidelines. All animal procedures were performed in accordance with institutional guidelines and approved by the Institutional Animal Care and Use Committee (IACUC) of University of California at Davis. B-cell lymphoma xenograft mouse model was established by subcutaneous implantation of Raji cells (1×10^7) at the right flank.

2.4 Cell uptake

Raji and Ramos cells were incubated with various DOX formulations (10 μM) at 37 °C for different period of time (30 min or 2 h), respectively. Then, cells were washed with PBS, spun down onto glass slides, fixed with 4% paraformaldehyde, stained by DAPI, and observed under confocal fluorescence microscopy (Olympus FV1000).

In another experiment, after the same exposure of DOX formulations as above, cells were subjected to the flow cytometric analysis (FACScan, Becton Dickinson), and 10, 000 events were collected for each sample.

2.5. In vitro cytotoxicity assay

The *in vitro* cytotoxicity of DOX formulaitons againt B-cell lymphoma cells was evaluated by MTS assay [21]. 4, 000 Raji or Ramos cells were seeded into a 96-well plate. After overnight, cells were incubated with different concentrations of free DOX, DOX nanoformulations, as well as the equivalent empty micells, respectively. At 72 h after incubation, the cell viability was measured by MTS assay.

2.6. Pharmacokinetics and biodistribution

BALB/c mice (n = 4) were injected intravenously with free DOX, DOX-NCMs, and DOX-DCMs at the dose of 10 mg/kg, respectively. Blood samples were collected in a heparinized tube *via* orbital vein at different time points post-injection. Plasma was isolated by centrifugation, and DOX was extracted for fluorescence detection as previously described [21]. Briefly, plasma was mixed with 9-fold volume of extraction buffer (10% Triton X-100, deionized water, and acidified isopropanol, 1:2:15), and DOX was extracted overnight at -20 °C. The DOX fluorescence in the supernatant was measured with the excitation of 470 nm and the emission of 590 nm. The standard curve of DOX in the blood was generated as previously reported [21]. Pharmacokinetic parameters such as distribution half-life ($T_{1/2\alpha}$), elimination half-life ($T_{1/2\beta}$), area under curve (AUC), clearance from the blood (CL), mean residence time (MRT), and steady-state volume of distribution (Vss) were calculated and analyzed by using DAS2.0 software.

In another independent experiment, Raji lymphoma bearing mice (n = 4) were injected with various DOX formulations (10 mg/kg), respectively. The animals were euthanized at 24 h, and major organs and tumor tissue were collected, weighed, and homogenized. Then, DOX was extracted and subjected to fluorescence detection as described above. The standard curve of DOX in each tissue was generated as previously reported [21]. The data was presented as the percentage of injected dose per gram tissue.

2.7. NIRF optical imaging

Raji lymphoma bearing nude mice (n = 3) were intravenously injected with DiD and DiD-loaded DCMs, respectively. At different time points post-injection, mice were anesthetized and imaged using IS2000MM Kodak imaging system (excitation = 625 nm, emission = 700 nm). At 48 h, the mice were euthanized, and major organs and tumor tissue were harvested for *ex vivo* imaging. To analyze the histological distribution of DCMs in tumor tissue,

excised tumors were cut into slices, fixed with 4% paraformaldehyde, stained with DAPI, and observed with confocal fluorescence microscopy (Olympus FV1000).

2.8. In vivo therapeutic studies

Subcutaneous Raji lymphoma bearing mice (n = 6–7) with the tumor volume of 100 – 200 mm^3 were administered intravenously with PBS, free DOX, DOX-NCMs, and DOX-DCMs (10 mg/kg) on day 0, 4, 8 and 12 for a total of 4 doses, respectively. Mice in another group of DOX-DCMs were also injected with NAC (10 mg/kg) at 24 h after each dose of DOX-DCMs. Tumor volume was measured by caliper twice per week, and calculated as length × width × width/2. Mice were euthanized for humane reasons when tumor volume reached 2000 mm^3, which was considered as the end point of survival data. Blood samples were collected at day 7 after the last dosage for complete cell count (CBC), serum chemistry analysis including creatine kinase (CK) and lactate dehydrogenase (LDH), which are the serum markers of cardiac toxicity.

2.9. Statistical analysis

Statistical analysis was performed by one-way analysis of variance (ANOVA) followed by Newman-Keuls test. Animal survival was analyzed by log-rank test using the GraphPad Prism software (GraphPad Software, Inc.). $P < 0.05$ was considered as statistical significance.

3. Results and discussion

3.1 Preparation and characterization of DOX-DCMs

DOX could be successfully encapsulated into the DCMs using the dry-down method. The loading efficiency of DOX into DCMs was almost 100% when the initial amount of added DOX was 3 mg or less in 20 mg PEG^{5k}-Cys_4-L_8-CA_8 telodendrimer, and decreased gradually when the added DOX was increased beyond 3 mg (Figure 1A). The intramicellar disulfide bond formation was monitored by Ellman's test, and the result (Figure S-2) demonstrated that more than 97% thiol group was converted in the micelles at 2 h after the addition of 1.5 equivalent H_2O_2. The final particle sizes of DOX-DCMs after filtration (0.22 μm) remained in the range of 15–20 nm (Figure 1B). The morphology of DOX-DCMs was observed under TEM and the result (Figure 1C) showed that DOX-DCMs (DOX loading at 2.9 mg/mL in 20 mg/mL telodendrimer) were spherical and uniform, with the average diameter of around 20 nm, which was in accordance with the results obtained from the DLS particle size analyzer (Figure 1D).

The stability of DOX-DCMs in physiological conditions was investigated by monitoring their particle size change after incubation with 50% human plasma. As shown in Figure 2B, the size distribution of DOX-DCMs remained uniform (~20 nm) after 24 h incubation, whereas the distribution of DOX-NCMs became less uniform, with two populations of larger size particles (363 nm and 2021 nm, Figure 2A), indicating the formation of large aggregates. The stability of DOX-DCMs in the known micelles-disrupting surfactant SDS (2.5 mg/mL) was also evaluated. As shown in Figure 2C and Figure S-3, the DOX-NCMs particle disappeared immediately with the addition of SDS, whereas the particle size of

DOX-DCMs under the same condition remained constant over a few days, indicating that DOX-DCMs still remained intact. However, in the presence of both SDS and reducing agents such as GSH (10 mM) or NAC (10 mM), the DOX-DCMs disintegrated suddenly after 20–25 min, indicating that rapid micelle dissociation did occur when most of the disulfide bonds in the micelles were reduced.

The DOX release characteristics from DOX-DCMs were measured by the dialysis method. As shown in Figure 2D, the drug release from free DOX was very fast, with almost 80% release within the first 4 h, whereas the micellar formulations (both NCMs and DCMs) significantly slowed down the rate of DOX release ($P < 0.05$). Meanwhile, DOX-DCMs released the drug more slowly than DOX-NCMs ($P < 0.05$). Furthermore, the addition of reducing agent such as GSH or NAC was able to accelerate the drug release of DOX-DCMs, suggesting that the fast DOX release from DOX-DCMs upon their tumor accumulation can be triggered by either the high concentration of endogenous GSH in cancer cells or the exogenous NAC, which is a FDA approved reducing agent.

3.2 Cellular uptake of DOX-DCMs

The uptake and intracellular distribution of DOX-DCMs in B-cell lymphoma cells were first observed under confocal microscopy.

intracellular uptake and distribution of DOX-DCMs in Raji lymphoma cells were qualitatively observed under confocal fluorescence microscopy. As shown in Figure 3A, all DOX formulations were able to be gradually internalized into Raji cells, with most of them (red fluorescence) distributed in the cytoplasm at 30 min. Interestingly, there were some fluorescent foci in the perinuclear region of DOX nanoformulations treated cells, which may be the micelles trapped in the endosomes or lysosomes. This indicates that DOX-NCMs and DOX-DCMs were internalized into the cells *via* the endocytosis pathway. At 2 h, most fluorescence from free DOX and DOX-NCMs were transported into the nuclei, while some fluorescence from DOX-DCMs still remained in the cytoplasm (Figure 3B), indicating the slower intracellular release of DOX from DCMs.

The cellular uptake of DOX formulations were also quantatively analyzed by flow cytometry. After 2 h incubation, the uptake of DOX-NCMs and DOX-DCMs in Raji (Figure 3C) and Ramos cells (Figure 3D) was significantly higher than that of free DOX, which is consistent with the notion that micelles may prevent the extracellular drug efflux and overcome the multiple drug resistance (MDR) associated with DOX [30].

3.3 In vitro cytotoxicity of DOX-DCMs

As shown in Figure 4, the cytotoxicity of DOX-DCMs against Raji and Ramos cells was similar to that of free DOX and DOX-NCMs, and their IC_{50} values were approximately within the range of 16 to 24 ng/mL. Meanwhile, no obvious cytotoxic effect was observed with empty DCMs up to 1 mg/mL, indicating the micelle-forming telodendrimer itself is biocompatible.

3.4 Pharmacokinetics and biodistribution

Plasma pharmacokinetic profile of free DOX and its micellar formulations is illustrated in Figure 5A. Pharmacokinetic parameters were calculated using DAS2.0 software and are presented in Table S-1. All three DOX formulations had a characteristic rapid decline distribution phase, and the distribution half-life ($T_{1/2\alpha}$) of free DOX, DOX-NCMs and DOX-DCMs were 1.8 ± 0.8 min, 3.2 ± 2.9 min, and 2.4 ± 0.6 min, respectively. After the initial rapid distribution phase, they continued to be eliminated from the blood. However, the elimination half-life ($T_{1/2\beta}$) of DOX-NCMs (5.0 ± 1.7 h) and DOX-DCMs (7.7 ± 2.1 h) were significantly longer than that of free DOX (1.4 ± 1.0 h). Meanwhile, the AUC of DOX-NCMs and DOX-DCMs were 6.1 times and 12.4 times higher than that of free DOX, respectively, and the Vss and CL of DOX-DCMs were significantly lower than that of free DOX ($P < 0.05$). These analyses suggested that micellar formulations especially DOX-DCMs remarkably prolonged the blood circulation time, and slowed down the elimination of DOX.

The biodistribution of DOX formulations in major tissues were further investigated in Raji tumor bearing mice at 24 h after administration (10 mg/kg). The DOX amount in each tissue was detected by fluorescence measurement, in view of the strong linear correlation between fluorescence intensity and DOX concentration demonstrated in our previous reports [21]. As shown in Figure 5B, micellar formulations significantly enhanced the DOX accumulation in tumor tissue ($P < 0.05$), and the tumor uptake of DOX-NCMs and DOX-DCMs were 1.6-fold, and 1.9-fold higher than that of free DOX, respectively. This can be attributed to the prolonged circulation and the EPR effect of micellar formulations [17, 20]. The increased uptake of both DOX-NCMs and DOX-DCMs in liver and spleen may be secondary to nonspecific capture by the reticular endothelial system [31]. Importantly, micellar formulations, especially DOX-DCMs, were able to significantly reduce the distribution of DOX drug to the heart tissue ($P < 0.05$), resulting in the attenuation of cardiotoxicity caused by DOX [32].

3.5 NIRF optical imaging

DiD, a NIRF probe, was encapsulated into DCMs to track, in real-time, the tumor targeting process of DCMs *in vivo*. As demonstrated in Figure 6A and Figure S-4A, no obvious tumor uptake was found in mice injected with free DiD dye, whereas DiD-DCMs were able to gradually accumulate at the tumor site starting from 1 h post-injection, and stayed over 48 h. *Ex vivo* images at 48 h (Figure 6B and Figure S-4B) further confirmed the preferential uptake of DiD-DCMs in the tumor tissue than other normal organs (except the liver where macrophages reside), which is in accordance with the aforementioned biodistribution results. Microscopic analysis demonstrated the fluorescence signal of DiD-DCMs was distributed throughout the tumor tissue, and was significantly higher than that of free DiD (Figure 6C).

3.6 In vivo anti-tumor efficacy study

Subcutaneous Raji lymphoma bearing nude mice were administered intravenously with PBS control, free DOX (10 mg/kg, MTD), DOX-NCMs (10 mg/kg) or DOX-DCMs (10 mg/kg) on days 0, 4, 8, and 12 for a total of 4 doses, respectively (n = 6–7). As shown in Figure 7A, all the DOX formulations significantly inhibited tumor growth compared to the PBS control

($P < 0.05$). However, micellar formulations improved the tumor growth inhibition (Figure 7A) and survival rate of DOX at the equivalent dose (Figure 7B). The median survival time of mice in the group of PBS control, free DOX, DOX-NCMs, and DOX-DCMs were 20, 32, 35, and 38 days, respectively. The enhanced anti-tumor efficacy of micellar formulations may be attributed to the higher amount of DOX delivered to the tumor site *via* the EPR effect [33]. Importantly, the therapeutic efficacy of DOX-DCMs was superior to that of DOX-NCMs, which may benefit from their improved colloidal stability, prolonged blood circulation, and enhanced tumor accumulation as demonstrated above. Furthermore, the subsequent administration of exogenous reducing agent NAC (FDA approved medications for the treatment of acetoaminophen overdose [34]) at 24 h further improved the anti-cancer efficacy of DOX-DCMs. This result indicates that the exogenous NAC might be able to precisely cleave the intra-micellar disulfide crosslinks of DCMs accumulated at the tumor site, and trigger the rapid release of DOX into the tumor microenvironment to kill cancer cells. This on-demand triggering release concept can probably be expanded to other stimuli-responsive drug delivery systems, and potentially be translated into clinical treatment in the future.

Toxicities were assessed by monitoring the body weight change, blood cell counts, and serum chemistry. Compared to the PBS control, all treatment led to the initial loss of body weight in animals to some extent, but the body weight loss in free DOX group (with the nadir of approximately 15%) was significantly higher than that in both micellar groups ($P < 0.05$, Figure 7C). After drug withdrawal, the body weight of mice in all the groups gradually recovered. CBC results demonstrated that the WBC count in free DOX group decrease significantly ($P < 0.05$) when compared to that in the PBS control group, whereas the WBC and other hematological parameters in the DOX-DCMs group were all within the normal ranges, which excludes their potential hematologic toxicity (Table S-2). Serum chemistry parameters such as ALT, AST, and BUN were within the normal ranges for all the treatment groups (Table S-3), indicating the absence of hepatic and renal toxicity, although some nonspecific uptake of DOX micellar formulations in the liver was observed in the above biodistribution results. Most importantly, the elevated levels of serum CK and LDH (two important biomarkers of cardiac toxicity) induced by free DOX were significantly decreased by the micellar formulations especially DOX-DCMs (Figure 8). This coincides with previous reports of DOX liposomal formulations, which are able to reduce the distribution of DOX to the heart, thus alleviating its cardiotoxicity [21].

Collectively, we have demonstrated DOX-DCMs not only achieved superior therapeutic efficacy against B-cell lymphoma, but also potentially attenuated DOX-induced cardiotoxicity. It is expected that the addition of cancer cell targeting ligands on the surface of DCMs will provide more accurate drug delivery to cancer cells, and further improve the therapeutic efficacy of delivered drugs. For instance, we have identified a lymphoma targeting ligand LLP2A with high affinity and high specificity obtained by one-bead one-compound (OBOC) combinatorial chemical screening [35]. We are planning to covalently conjugate LLP2A ligand to the distal terminus of the PEG chain of PEG^{5k}-Cys_4-L_8-CA_8 telodendrimer *via* click chemistry, and evaluate the active targeting effect and therapeutic efficacy of the resulting LLP2A-targeted DCMs against lymphoma.

4. Conclusion

In summary, we have successfully developed a novel reversibly disulfide crosslinked micellar formulation of DOX for the treatment of non-Hodgkin lymphoma. DOX could be efficiently encapsulated into DCMs, and the resulting DOX-DCMs exhibited optimal particle size, outstanding stability, and redox-responsive drug release properties. DOX-DCMs formulation significantly improved the pharmacokinetics and biodistribution profiles of DOX, such as prolonging its half-life, increasing its AUC, enhancing its tumor accumulation and reducing its cardiac distribution. DOX-DCMs were proved to be more efficacious than the equivalent dose of free DOX and non-crosslinked micellar formulation in B-cell lymphoma xenograft model, and significantly reduced the DOX-mediated cardiotoxicity. Furthermore, the administration of exogenous reducing agent NAC further improved the therapeutic efficacy of DOX-DCMs by on-demand triggering drug release at the tumor site.

Supplementary Material

Refer to Web version on PubMed Central for supplementary material.

Acknowledgments

The authors thank the financial support from NIH/NCI (R01CA199668 & 3R01CA115483), NIH/NIBIB (5R01EB012569), NIH/NICHD (1R01HD086195), DoD PRMRP Award (W81XWH-13-1-0490), and National Natural Science Foundation of China (81101143 & 81572617).

References

1. Outomuro D, Grana DR, Azzato F, Milei J. Int J Cardiol. 2007; 117:6–15. [PubMed: 16863672]
2. Tacar O, Sriamornsak P, Dass CR. J Pharm Pharmacol. 2013; 65:157–170. [PubMed: 23278683]
3. Park J, Fong PM, Lu J, Russell KS, Booth CJ, Saltzman WM, Fahmy TM. Nanomedicine. 2009; 5:410–418. [PubMed: 19341815]
4. Khawar IA, Kim JH, Kuh HJ. J Control Release. 2014; 201:78–89. [PubMed: 25526702]
5. Sharma G, Anabousi S, Ehrhardt C, Kumar MNVR. Journal of Drug Targeting. 2006; 14:301–310. [PubMed: 16882550]
6. Fukumori Y, Ichikawa H. Advanced Powder Technology. 2006; 17:1–28.
7. Gillies ER, Frechet JMJ. Drug Discovery Today. 2005; 10:35–43. [PubMed: 15676297]
8. Lukyanov AN, Torchilin VP. Advanced Drug Delivery Reviews. 2004; 56:1273–1289. [PubMed: 15109769]
9. Yardley DA. J Control Release. 2013; 170:365–372. [PubMed: 23770008]
10. Markman JL, Rekechenetskiy A, Holler E, Ljubimova JY. Adv Drug Deliv Rev. 2013; 65:1866–1879. [PubMed: 24120656]
11. Barenholz Y. J Control Release. 2012; 160:117–134. [PubMed: 22484195]
12. O'Brien ME, Wigler N, Inbar M, Rosso R, Grischke E, Santoro A, Catane R, Kieback DG, Tomczak P, Ackland SP, Orlandi F, Mellars L, Alland L, Tendler C. Ann Oncol. 2004; 15:440–449. [PubMed: 14998846]
13. Mian M, Wasle I, Gamerith G, Mondello P, Melchardt T, Jager T, Linkesch W, Fiegl M. Clinical oncology. 2014; 26:648–652. [PubMed: 24929649]
14. Andresen TL, Jensen SS, Jorgensen K. Prog Lipid Res. 2005; 44:68–97. [PubMed: 15748655]
15. Luo J, Xiao K, Li Y, Lee JS, Shi L, Tan YH, Xing L, Holland Cheng R, Liu GY, Lam KS. Bioconjug Chem. 2010; 21:1216–1224. [PubMed: 20536174]

16. Gaucher G, Dufresne MH, Sant VP, Kang N, Maysinger D, Leroux JC. J Control Release. 2005; 109:169–188. [PubMed: 16289422]
17. Xiao K, Luo J, Fowler WL, Li Y, Lee JS, Xing L, Cheng RH, Wang L, Lam KS. Biomaterials. 2009; 30:6006–6016. [PubMed: 19660809]
18. Li Y, Xiao K, Luo J, Lee J, Pan S, Lam KS. J Control Release. 2010; 144:314–323. [PubMed: 20211210]
19. Xiao K, Li Y, Luo J, Lee JS, Xiao W, Gonik AM, Agarwal RG, Lam KS. Biomaterials. 2011; 32:3435–3446. [PubMed: 21295849]
20. Li Y, Xiao K, Luo J, Xiao W, Lee JS, Gonik AM, Kato J, Dong TA, Lam KS. Biomaterials. 2011; 32:6633–6645. [PubMed: 21658763]
21. Xiao K, Luo J, Li Y, Lee JS, Fung G, Lam KS. J Control Release. 2011; 155:272–281. [PubMed: 21787818]
22. Li Y, Xiao W, Xiao K, Berti L, Luo J, Tseng HP, Fung G, Lam KS. Angew Chem Int Ed Engl. 2012; 51:2864–2869. [PubMed: 22253091]
23. Xiao K, Li Y, Lee JS, Gonik AM, Dong T, Fung G, Sanchez E, Xing L, Cheng HR, Luo J, Lam KS. Cancer Res. 2012; 72:2100–2110. [PubMed: 22396491]
24. Kato J, Li Y, Xiao K, Lee JS, Luo J, Tuscano JM, O'Donnell RT, Lam KS. Mol Pharm. 2012; 9:1727–1735. [PubMed: 22530955]
25. Li Y, Xiao K, Zhu W, Deng W, Lam KS. Adv Drug Deliv Rev. 2013; 66:58–73. [PubMed: 24060922]
26. Xiao K, Suby N, Li Y, Lam KS. Ther Deliv. 2013; 4:1279–1292. [PubMed: 24116912]
27. Rijcken CJ, Snel CJ, Schiffelers RM, van Nostrum CF, Hennink WE. Biomaterials. 2007; 28:5581–5593. [PubMed: 17915312]
28. Xiao K, Li YP, Wang C, Ahmad S, Vu M, Kuma K, Cheng YQ, Lam KS. Biomaterials. 2015; 67:183–193. [PubMed: 26218744]
29. Koo AN, Lee HJ, Kim SE, Chang JH, Park C, Kim C, Park JH, Lee SC. Chem Commun (Camb). 2008:6570–6572. [PubMed: 19057782]
30. Zhou Y, Wang S, Ying X, Wang Y, Geng P, Deng A, Yu Z. International journal of nanomedicine. 2017; 12:6153–6168. [PubMed: 28883726]
31. Bai F, Wang C, Lu Q, Zhao M, Ban FQ, Yu DH, Guan YY, Luan X, Liu YR, Chen HZ, Fang C. Biomaterials. 2013; 34:6163–6174. [PubMed: 23706689]
32. Blank N, Laskov I, Kessous R, Kogan L, Lau S, Sebag IA, Gotlieb WH, Rudski L. Cancer chemotherapy and pharmacology. 2017; 80:737–743. [PubMed: 28801766]
33. Matsumura Y, Maeda H. Cancer Res. 1986; 46:6387–6392. [PubMed: 2946403]
34. Wong A, Landersdorfer C, Graudins A. European journal of clinical pharmacology. 2017; 73:1103–1110. [PubMed: 28624886]
35. Peng L, Liu R, Marik J, Wang X, Takada Y, Lam KS. Nature chemical biology. 2006; 2:381–389. [PubMed: 16767086]

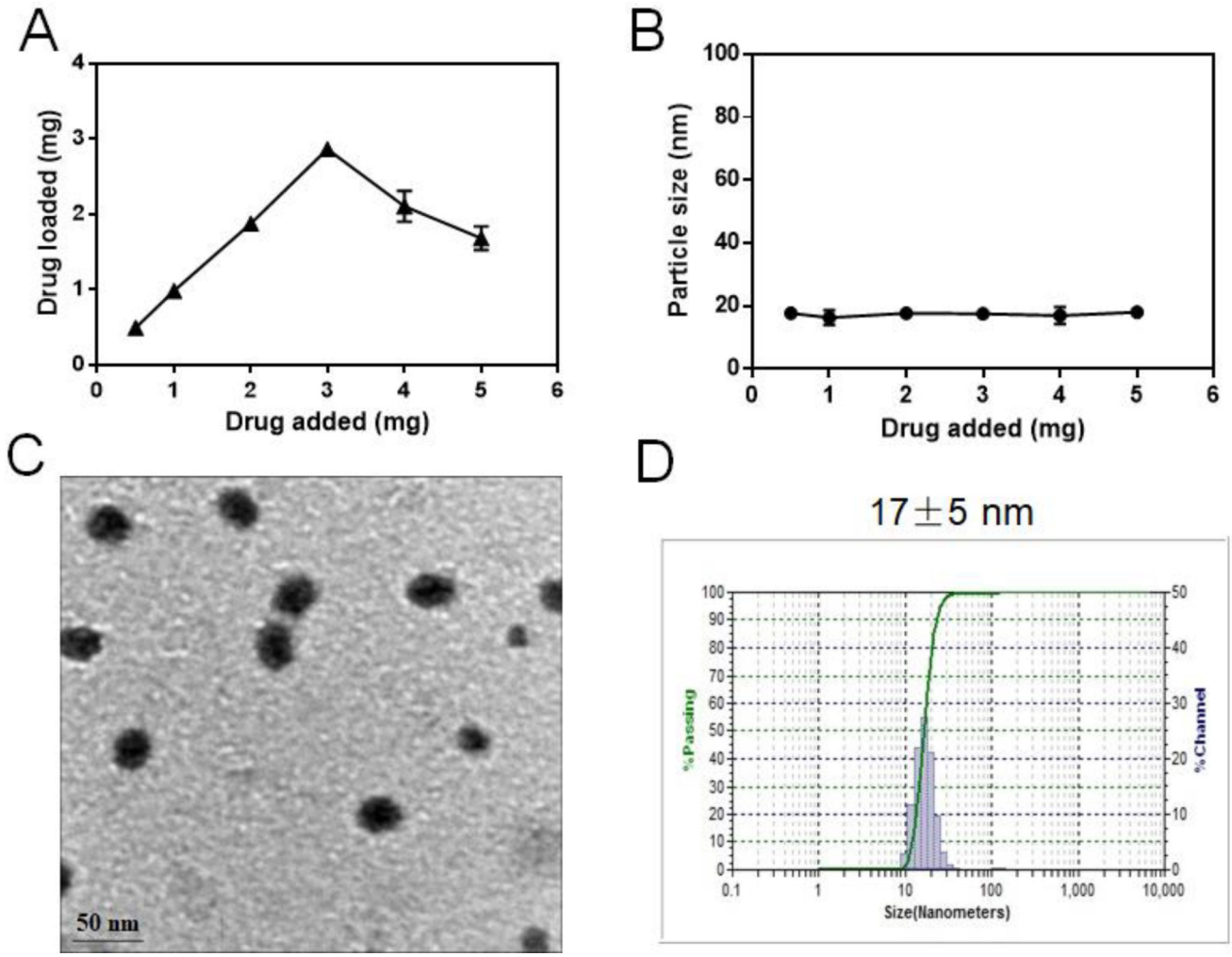

Figure 1.

Drug loading (A) and particle size (B) of PEG^{5k}-Cys_4-L_8-CA_8 disulfide cross-linked micelles (DCMs) versus the level of DOX drug added at initial loading. The final concentration of the telodendrimer was kept at 20 mg/mL. TEM image (C) and DLS size distribution (D) of DOX-DCMs (DOX loading was 2.9 mg/mL, TEM scale bar: 50 nm).

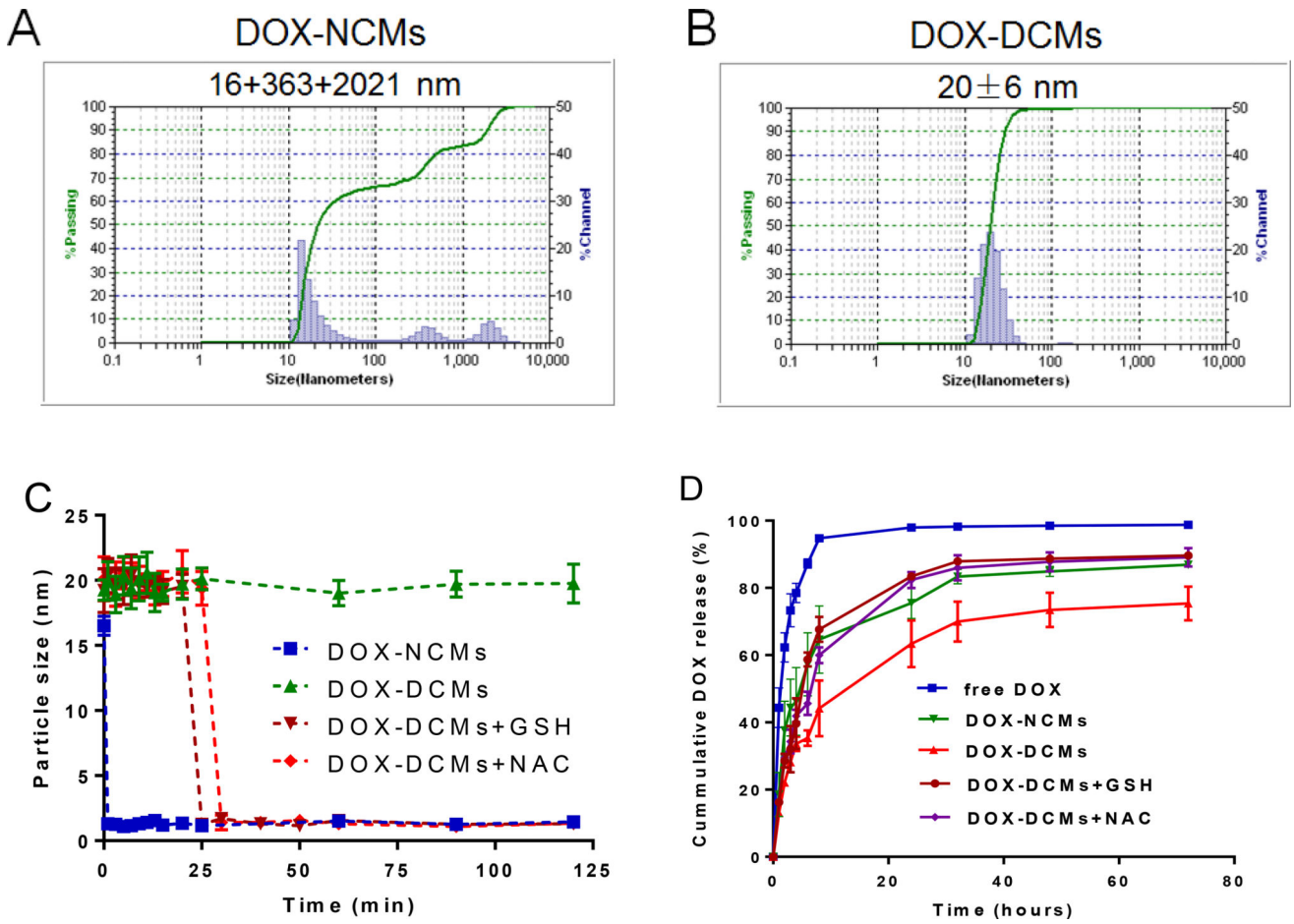

Figure 2.

The DLS particle size of DOX-NCMs (A) and DOX-DCMs (B) incubated with human plasma 50% (v/v) for 24 h at 37 °C. Drug loading level was 1.0 mg/mL DOX in 20 mg/mL telodendrimer. (C) The stability of DOX-NCMs and DOX-DCMs in the presence of 2.5 mg/mL SDS with or without N-acetylcysteine (NAC, 10 mM), Glutathione (GSH, 10 mM), by monitoring particle size change with DLS measurement. (D) Cumulative drug release profiles from free DOX, DOX-NCMs and DOX-DCMs measured by dialysis against PBS with activated charcoal at 37 °C.

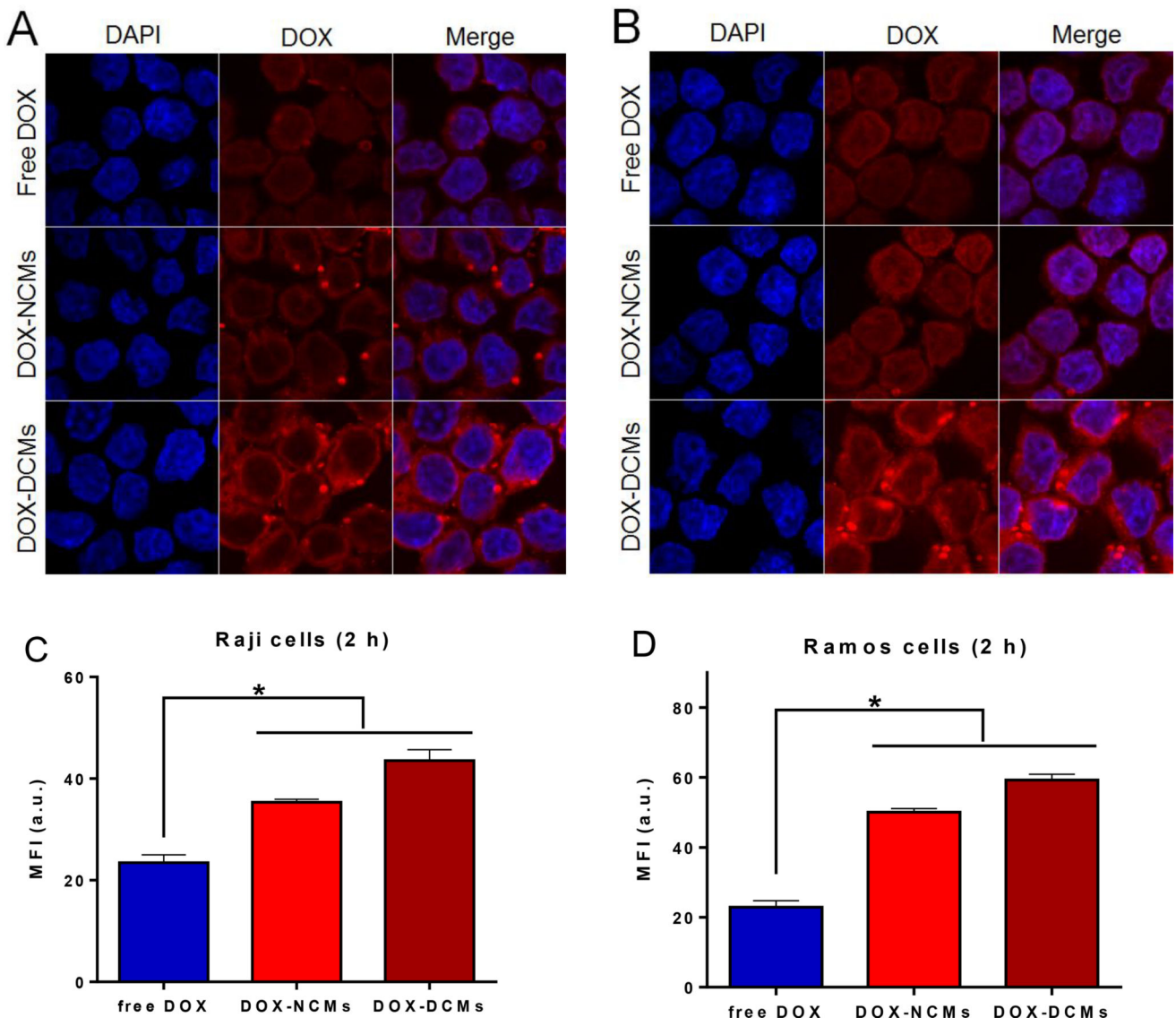

Figure 3.

Cellular uptake of DOX-DCMs in B-cell lymphoma cells. Representative confocal images of Raji cells incubated with 10 μM of free DOX, DOX-NCMs, and DOX-DCMs for 30 min (A) and 2 h (B), respectively. 40×magnification. Flow cytometric analysis of DOX uptake in Raji cells (C) and Ramos cells (D) after 2 h incubation with free DOX, DOX-NCMs, and DOX-DCMs.

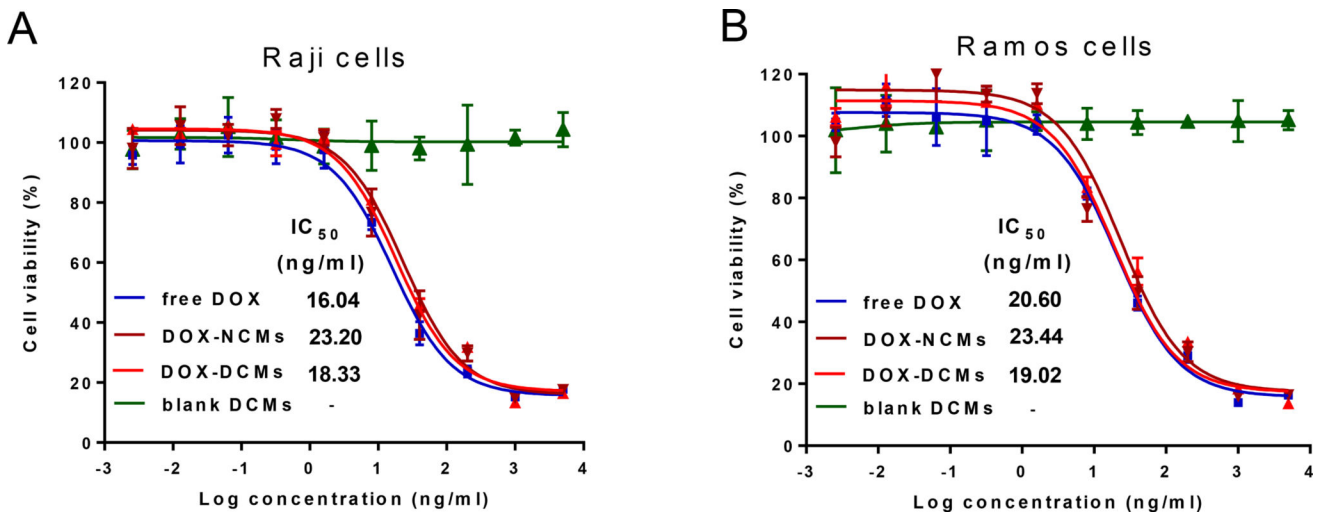

Figure 4.

The cell viability of Raji (A) and Ramos (B) B-cell lymphoma cell lines after 72 h incubation with free DOX, DOX-NCMs, DOX-DCMs, and blank DCMs

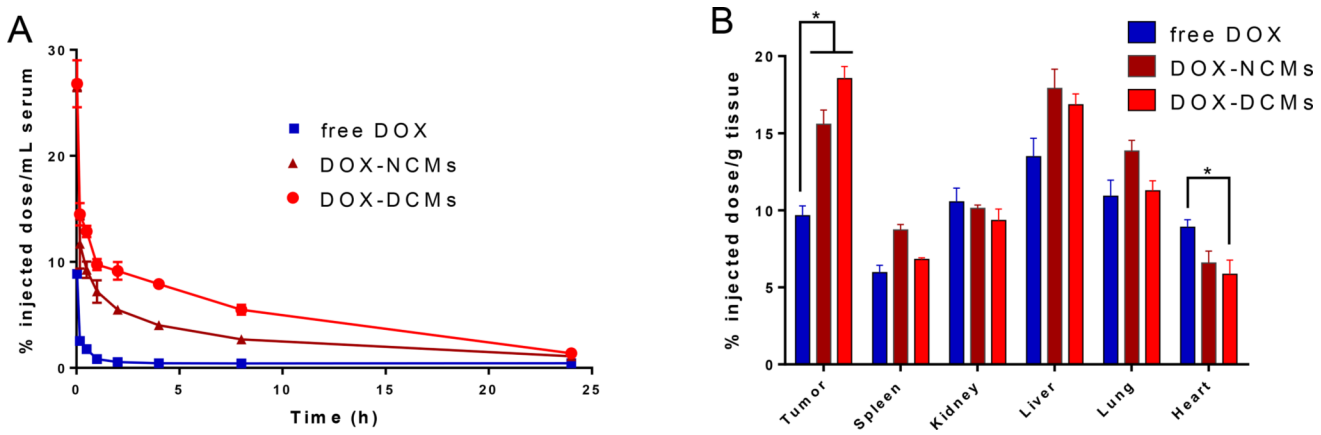

Figure 5.

Pharmacokinetics (A) and biodistribution (B, at 24 h post-injection) of free DOX, DOX-NCMs, and DOX-DCMs given intravenously at a dose of 10 mg/kg in Raji lymphoma bearing mice. * $P < 0.05$.

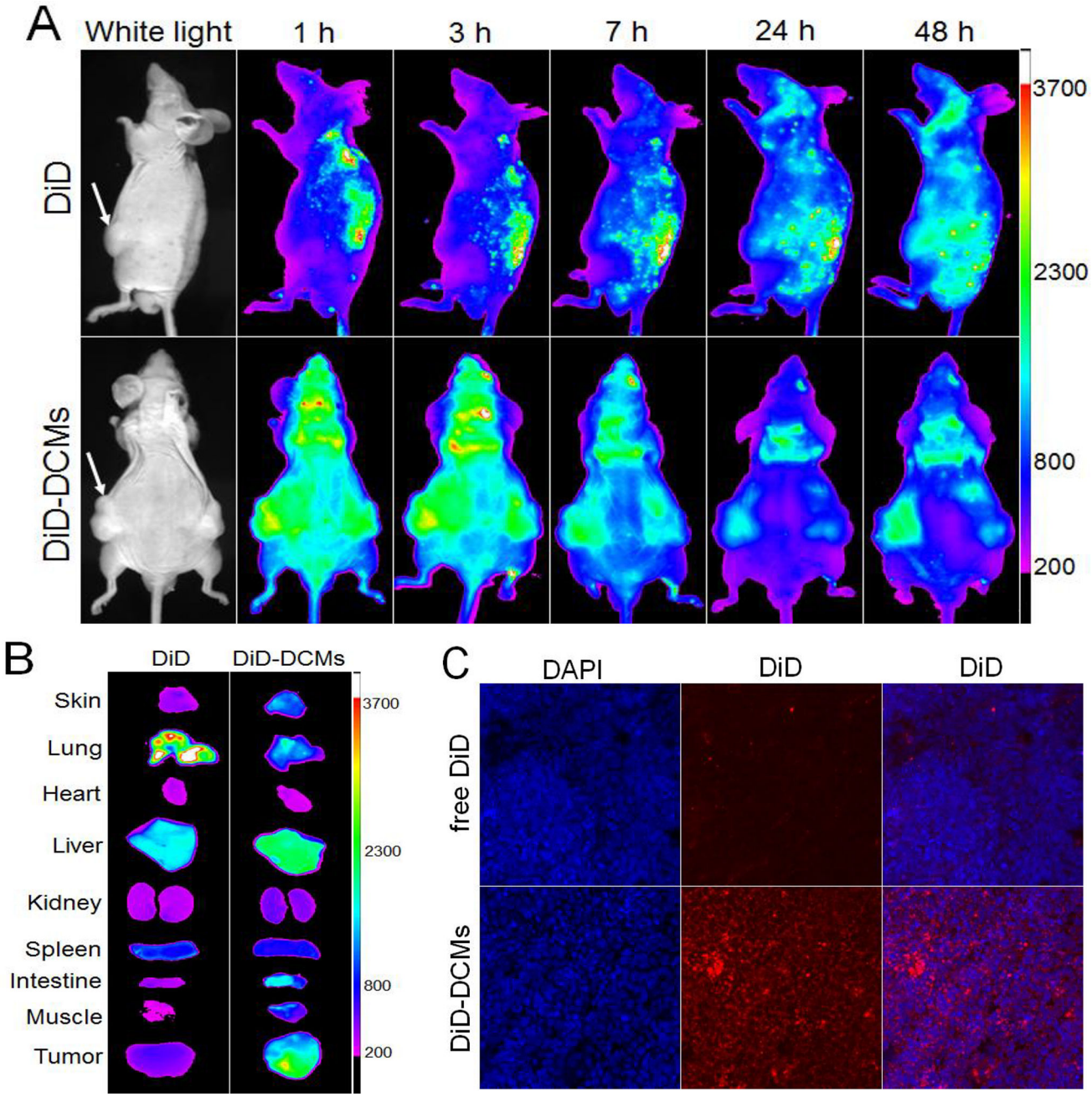

Figure 6.

In vivo (A) and *ex vivo* (B) NIRF images of Raji lymphoma bearing mice injected intravenously with free DiD dye and DiD-loaded DCMs, respectively. Tumors and major organs were excised for *ex vivo* imaging at 48 h post-injection. (C) Microscopic distribution of fee DiD or DiD-DCMs (red) in tumor cryo-sections. The nuclei were stained by DAPI (blue). 10×magnification.

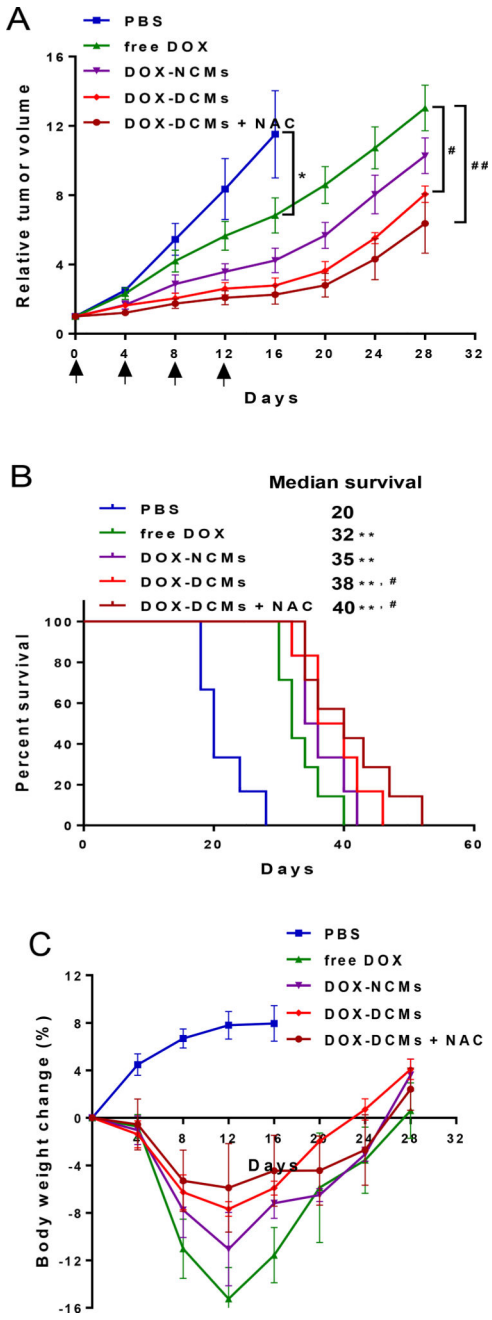

Figure 7.

In vivo tumor growth inhibition (A), Kaplan-Meier survival curve (B), and body weight changes (C) of B-cell lymphoma bearing mice treated with various DOX formulations. Nude mice bearing Raji lymphoma xenograft (n=6–7) were intravenously administrated with PBS, free DOX, DOX-NCMs and DOX-DCMs at the dose of 10 mg/kg, respectively. The dosage was given every four days for a total of 4 doses. N-acetyl cysteine (NAC) was also intravenously injected at 24 h after each dose to trigger drug release for another group of mice treated with DOX-DCMs. * $P < 0.05$, ** $P < 0.01$ compared with the PBS group; $^{\#}$ $P < 0.05$, $^{\#\#}$ $P < 0.01$ compared with free DOX group.

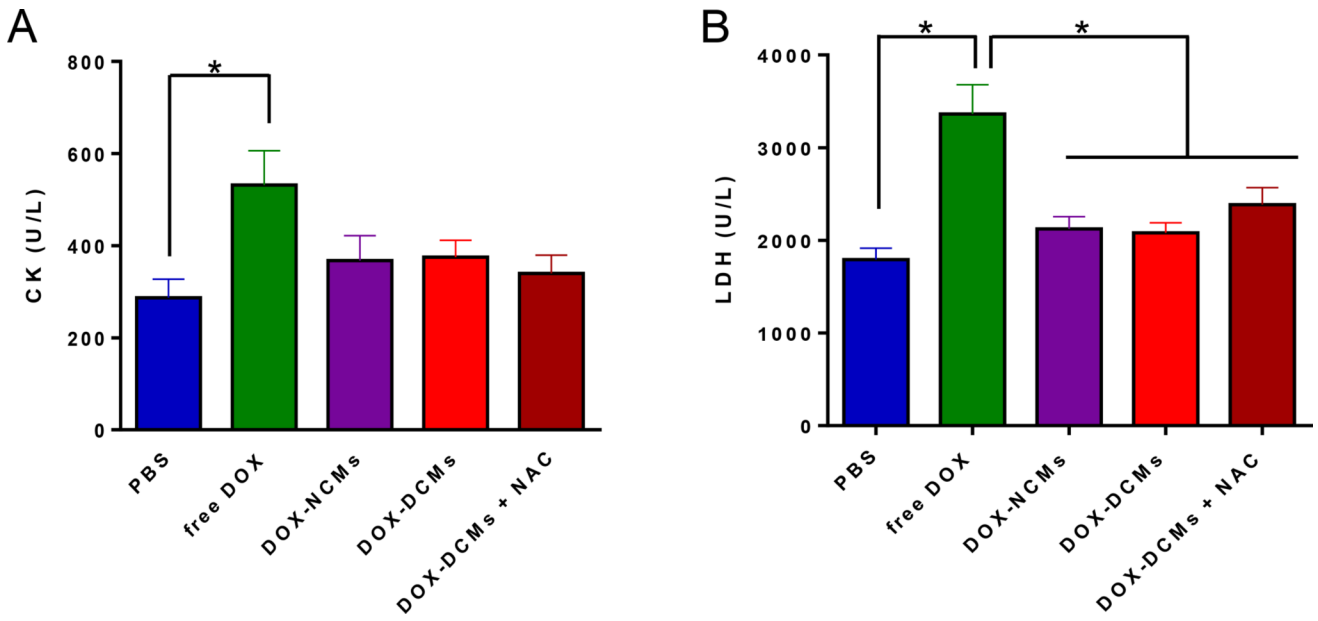

Figure 8.

The levels of serum creatine kinase (CK, A) and lactate dehydrogenase (LDH, B) on day 7 after the last dosage of treatment in Raji tumor bearing mice. Each data point is represented as mean ± SEM. * $P < 0.05$.